PHYSICAL REVIEW B **75**, 081404(R) (2007)

Role of surface peroxo and superoxo species in the low-temperature oxygen buffering of ceria: Density functional theory calculations

Min Huang and Stefano Fabris
SISSA and INFM DEMOCRITOS National Simulation Center, Via Beirut 2-4, I-34014 Trieste, Italy
(Received 19 January 2007; published 22 February 2007)

Reversible oxygen release makes ceria (CeO_2) among the most efficient oxide supports for low-temperature oxidation reactions. A clear identification of the species responsible for this oxygen buffering is still missing since only indirect information is available. We present a systematic study of O adsorbates on the most stable ceria surfaces based on density functional theory calculations. The results rationalize the experimental findings supporting the interpretation that superoxide species are the key factors in promoting low-temperature oxidation reactions on ceria. The high reactivity of nanocrystalline ceria is explained in terms of the surface selectivity towards superoxide adsorption.

DOI: 10.1103/PhysRevB.75.081404 PACS number(s): 68.47.Gh, 68.43.−h, 71.15.Mb

Oxide-supported noble-metal nanoparticles have been shown to efficiently promote low-temperature oxidation reactions.[1] Their reactivity is controlled by the presence of metal ions,[2] often nucleated at surface defects,[3] as well as by the active role of reducible-oxide supports in supplying reactive oxygen,[4] effectively acting as oxygen buffers. Ceria-based materials are among the most efficient of these active supports: The origin of their unique oxygen buffering capacity is often traced back to facile oxygen vacancy formation and surface reduction.[5] At high temperatures ($T>500\,^{\circ}C$), oxidation reactions involve lattice oxygen resulting from O vacancy formation and surface reduction, while at low temperatures ($T<200\,^{\circ}C$) surface O adspecies are involved.[4] The defective surfaces resulting from O release have been recently studied in detail,[6–9] but the O adsorbates relevant in the low-temperature O buffering are not easily accessible by local scanning techniques with the same high spatial resolution. As a result, the oxygen adspecies relevant in this process are not clearly characterized and, more generally, a fundamental understanding of the mechanisms by which O is released and exploited in the low-temperature oxidations on oxide supports is missing.

Spectroscopic studies on Au/CeO_2 catalysts suggest that the reactive oxygen supplied at the active sites during CO oxidation at low temperature (below 200 °C) might not be in the form of neutral atoms or O_2 molecules (resulting from oxygen vacancy formation), but rather in the form of charged adspecies.[4] These radicals may act as important intermediates in catalytic oxidations,[10] and can be particularly relevant in the context of many technologically important reactions, like low-temperature water gas shift or CO oxidation.[4,11] Charged adspecies may result from redox reactions, activated, for example, by the supported noble metals whose reactivity has been related to the formation of metal ions,[2] but the precise nature of the O adspecies reactive at low temperature remains unclear.

In this study, the oxygen adspecies relevant in the low-temperature O buffering property of ceria are identified via a systematic analysis based on density functional theory (DFT) calculations. To this end, we consider neutral (atomic and molecular) as well as charged oxygen species adsorbed on different surface sites, such as $CeO_2(111)$ and (110) terraces, one electron defects (Ce^{3+} ions isolated on the CeO_2 surface), two electron defects (neutral oxygen vacancies), and fully reduced $Ce_2O_3(0001)$ surfaces. The energies, electronic structures, and the adsorbate stretching frequencies resulting from the calculations allow us to rationalize the experimental finding and to identify superoxide species as key factors in controlling oxidation reactions.

The calculations are based on the DFT with the Perdew-Burke-Ernzerhof generalized gradient corrected approximation (GGA) for the exchange and correlation functional in the framework of ultrasoft pseudopotentials and plane waves as implemented in the Quantum-ESPRESSO computer package.[12] The wave function and electron density representation were limited by kinetic energies of 30 and 300 Ry, respectively. The $CeO_2(111)$, (110), and $Ce_2O_3(0001)$ surfaces were modeled with (2×2) supercells (nine, six, and ten layers thick, correspondingly), and separated by more than 10.9 Å of vacuum. The upper half of the supercells (containing the adsorbates) were fully relaxed. Brillouin-zone integration was performed on a $(2\times2\times1)$ Monkhorst-Pack grid conveying total-energy convergence to less than 0.03 eV. A value of Gaussian smearing of 0.07 eV was used in the calculations, and the reported results were extrapolated to 0 eV smearing. Charged adsorbates were simulated by including a uniform compensating background. Energy barriers and transition states for diffusion were calculated with the nudged elastic band (NEB) method.[13] Reduced ceria was modeled with the GGA+U method.[9,14] Since GGA and GGA+U calculations provide the same description of nondefective surfaces (differences in GGA and GGA+U binding energy are below 0.03 eV), only the GGA results will be reported in this case. Further calculation details can be found in Ref. 8. The stretching frequencies of the adsorbates were calculated with the frozen phonon method.

The binding energy E_{bind} of neutral adsorbates is calculated in terms of total energies of supercells containing (i) the adsorbate in the gas phase E_{ads}^{gas}, (ii) the clean surface E_{surf}, and (iii) the surface and the adsorbate $E_{ads/surf}$: $E_{bind}=(E_{ads}^{gas}+E_{surf})-E_{ads/surf}$. For charged adsorbates, the term in parentheses is calculated as the total energy of the supercell containing both the surface and the molecule, the latter being in the middle of the vacuum region, i.e., at 5.45 Å from the

TABLE I. (Color online) Binding energies, energy barriers for diffusion (estimated values displayed in gray boxes), and superoxide stretching frequencies for the adsorption of atomic O, molecular O_2, and superoxide O_2^- species on the flat CeO_2(110) and (111) terraces, on a (111) surface O vacancy site, on an isolated Ce^{3+} ion, and on a Ce^{3+} ion of the Ce_2O_3(0001) surface.

			O		O_2		O_2^-	
			E_{bind} [eV]	E_{diff} [eV]	E_{bind} [eV]	E_{diff} [eV]	E_{bind} [eV]	ω [cm^{-1}]
(110)	CeO_2	GGA	2.61	1.70	~0.03	-	1.10	1139
(111)	CeO_2	GGA	2.47	1.42	~0.01	-	0.17	1163
	O-vacancy	GGA+U	5.08	-	1.72	1.42	2.74	
	Ce^{3+} on CeO_2	GGA+U	2.23	~1.4	0.09	>0.4		
(0001)	Ce_2O_3	GGA+U	2.32	~1.4	0.08			

surface. Increasing this distance to 6.6 Å conveys differences in binding energy below 0.06 eV. Each of the binding energies reported in Table I refers to the corresponding adsorbate in the gas phase. Zero-point energy and entropic effects are not included in the reported binding energies and barriers. In the following, adsorbate O atoms will be denoted as O^*.

An O^* adatom binds to a surface O atom of a flat CeO_2(111) terrace by forming a characteristic spin unpolarized peroxo unit tilted by 60° with respect to the surface normal and with an O-O^* bond length of 1.44 Å [Fig. 1(a)]. The O^* atom lays on a bridge position with respect to two Ce atoms of the second layer. This adsorption geometry is almost degenerate with the metastable configuration (0.02 eV higher in energy) resulting from the rotation of the peroxo group by 60° around the surface normal centered on the surface O atom. In this metastastable configuration, the O^*-O bond length and the spin magnetic moment are unchanged with respect to the lowest energy ones. The bonding charge density clearly shows that the charge redistribution due to O adsorption involves only the O^* and the neighboring surface O atom [Fig. 1(a)]. The Löwdin charges of these two atoms are equal. Similar peroxide species have been recently identified on the surfaces of alkaline-earth oxides.[15,16] The adsorption of atomic oxygen on ceria does not modify the occupancy of the Ce-4*f* states, therefore GGA and GGA+*U* calculations provide equivalent descriptions of the process. The binding energy with respect to atomic oxygen is large, 2.47 eV for the lowest energy configuration (Table I). The same peroxo unit is also formed on the (110) surface, with an equally large binding energy of 2.61 eV (Table I).

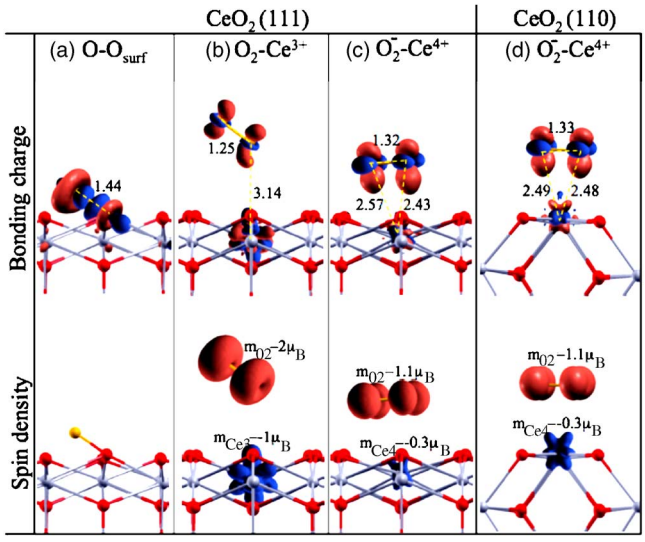

FIG. 1. (Color online) Bonding charge (top panels) and spin (bottom panels) densities for (a) an O adatom bound to the nondefective (111) surface, (b) molecular oxygen adsorbed on a one-electron Ce^{3+} defect of the (111) surface, and a superoxide molecule bound to a Ce^{4+} ion of the (c) (111) and (d) (110) surfaces. Relevant bonding distances (in Å, top panels), and spin polarizations (in μ_B, bottom panels) are also shown. Red (dark gray) and light gray spheres represent surface O and Ce atoms, respectively, while adsorbates are displayed in yellow (light gray). Positive and negative density values are displayed in red (lighter gray) and blue (darker gray), respectively.

Two fundamental mechanisms control the O^* mobility on the most stable (111) surface: the rotation of the peroxo unit around the given surface O atom and the actual diffusion of the O^* adatom on the surface. The energy barrier for rotation is only 0.02 eV. The peroxo unit is therefore free to rotate with virtually no energy cost. The energy barrier for adatom diffusion is 1.42 eV and the adsorbate spin is conserved during diffusion (in all configurations, the initial spin of the O^* adatom was unconstrained during the self-consistent procedure and always resulted in a spin unpolarized system). This large activation energy suggests that, once the peroxide unit has been formed, the O^* adatom is unlikely to diffuse except at high temperatures. A similar high barrier (1.70 eV, Table I) for the direct O adatom diffusion has been identified on the (110) surface, but in this case the adsorbate spin is not conserved along the path resulting from the NEB calculation.

The actual diffusion mechanism is therefore likely to be different from the (111) case, probably similar to the one proposed for the MgO (001) surface,[15] involving first the spin polarization of the adatom and then the diffusion along the spin-polarized path. Overall, once bound into the peroxide unit, the mobility of the O^* adatoms around room temperature is therefore very low, and will be activated only at temperatures larger than 300–400 °C.

The effect of an O vacancy on the adsorption of an O^* atom is very local, being limited to the first rim of neighboring surface O atoms. When an O^* atom is placed inside the rim it is readily attracted by the electrostatic field of the vacancy, resulting in vacancy annihilation and surface re-oxidation. The binding energy at a vacancy site of the (111) surface is 5.08 eV (Table I). Binding to a surface O atom of the rim results in the formation of the peroxo unit described above and in a binding energy of 2.49 eV, quite close to the asymptotic value for an O^* atom on an oxidized flat terrace (2.47 eV). The process of vacancy annihilation by an adsorbed O^* atom is also strongly exothermic (2.67 eV), but despite this large driving force, re-oxidation is probably hindered by the large energy barrier for diffusion (1.42 eV). As a result, peroxo units are likely to be present at low temperature also on partially reduced surfaces as metastable adsorbates.

Adsorption of an O^* atom to a surface O atom close to a one-electron defect (an isolated Ce^{3+} ion) of the $CeO_2(111)$ or of the $Ce_2O_3(0001)$ surfaces results in the formation of the same O^*-O peroxo unit described above, with slightly lower binding energies, 2.23 and 2.32 eV, respectively (Table I). We can therefore estimate that the energy for O^* diffusion on these surfaces is likely to be similarly large ($\approx$1.4 eV) as the one on the oxidized $CeO_2(111)$ flat terrace. Overall, O adatoms forming the peroxo units are relevant as reaction intermediates in the surface chemistry of ceria, but, due to their high diffusion barrier, their dynamic role in promoting low-temperature oxidations on ceria surfaces is predicted to be minor.

Molecular O_2 physisorbs very weakly on the flat nondefective surfaces. Our estimate of E_{bind}=0.01–0.03 eV (Table I) does not include van der Waals contributions, which are known to be important in this weak physisorption regime, but is, however, consistent with Raman spectroscopy data on oxidized ceria surfaces. These measurements[11] show that the characteristic frequency of adsorbed molecular O_2 (1551 cm^{-1}) is present only below 153 K. Defective surfaces are reoxidized by O_2 molecules, forming the strongly bound and immobile peroxo units described above. The driving force for this oxidation reaction with respect to a free O_2 molecule is 1.72 eV (Table I). Molecular oxygen binds stronger above one-electron defects, E_{bind}=0.09 eV (Table I). The bonding does not involve charge transfer between the adsorbate and the surface. The O^*-O^* bond length (1.25 Å), as well as the magnetic moments of the O_2 molecule and of the Ce^{3+} ion are unaffected upon adsorption [Fig. 1(b)]. The diffusion of this O_2-Ce^{3+} unit is likely to be controlled by electron hopping between neighboring Ce sites. We thus assume the energy barrier for diffusion to be close to the activation energy for polaron electron transport in bulk, $\approx$0.4 eV.[17] This value is larger than the binding energy, therefore the direct diffusion of these species is unlikely and, given the very low binding energy, they can exist on partially reduced surfaces only at very low temperatures.

Charged superoxide O_2^- species adsorb on hollow sites of the (111) surface, above a Ce^{4+} ion, in a side-on configuration [Fig. 1(c)]. The calculated spin polarization and the O^*-O^* bond length (1.36 Å) are compatible with those of a free superoxide (1.35 Å, Ref. 18). The superoxide adsorbate is located at 1.78 Å over the surface O atoms and forms two O^*-Ce bonds at 2.43 and 2.57 Å. The Ce ion bound to the adsorbate relaxes outward by 0.20 Å. The binding energy with respect to free molecular superoxide is 0.17 eV (Table I). The spin density is mostly distributed on the superoxide molecule, but the underlying Ce ion is also weakly polarized [Fig. 1(c)]. The occupancy of the Ce 4*f* states is not modified in the adsorption process. A metastable end-on adsorption configuration, almost degenerate with the side-on one, has been also identified (0.04 eV higher in energy). This is in agreement with spectroscopic studies showing that both end-on and planar geometries can be present on ceria surfaces.[11] A similar adsorption configuration has been identified also on the (110) surface [Fig. 1(d)], but here the binding energy is larger, 1.10 eV (Table I), resulting from the stronger electrostatic interaction with the more exposed Ce^{4+} ions. Finally, on the (111) surface, the driving force for vacancy annihilation by these superoxide radicals is 2.74 eV, leading to the peroxide units on the one-electron Ce^{3+} defects described above.

Direct experimental characterization of the O adsorbates involved in oxidation reactions is missing, but the measured vibrational frequencies, $\approx$1123–1135 cm^{-1},[4,11] are consistent with those of superoxide species, whose frequency in vaccum is 1108 cm^{-1} (Ref. 18) (the corresponding calculated value is 1117 cm^{-1}). By this analogy, these frequencies have been tentatively associated to superoxide species adsorbed to Ce^{4+} sites. We have calculated the stretching frequency of the superoxide radicals adsorbed on the (111) and (110) surfaces to be 1163 and 1139 cm^{-1}, respectively. The calculated frequency shift upon adsorption (22–46 cm^{-1}) is larger than the measured one (15–27 cm^{-1}), but in overall good agreement with the experimental values, hence allowing for a direct interpretation of these frequencies.

Moreover, the calculated weak binding energies of 0.17 eV are consistent with the Raman spectra[11] showing that these superoxide species are not stable even at room temperature on pure polycrystalline CeO_2 samples, which are known to expose almost exclusively (111) surfaces. The frequencies at 1123–1135 cm^{-1} are present only below 213 K on polycrystalline ceria,[11] but are observed up to $\approx$470 K on nanocrystalline Au/CeO_2 samples,[4] which expose a larger fraction of (110) surfaces. Besides the presence of the supported metal, this increase in stability of superoxide adsorbates up to technologically relevant temperatures is determined by the strong surface selectivity predicted by the calculations, resulting from the larger fraction of exposed Ce^{4+} ions in nanocrystalline samples.

The interplay between the O_2-Ce^{3+} and O_2^--Ce^{4+} species, together with the presence of supported metal atoms, opens up new possibilities for the participation of adsorbed O_2 in

oxidation reactions and is controlled by the possibility to reduce the Ce ions. In the specific case of pure (111) surface, the O_2^--Ce^{4+} is predicted to be a reactive intermediate, since the O_2-Ce^{3+} unit is more stable by 0.2 eV, but in general, the presence of one or the other unit is likely to be determined by the local mechanism of superoxide formation (the specific redox couple), by the presence of adsorbed metal atoms, by the degree of reduction of the surface, and by the activation barrier for the electron transfer transforming one unit in the other.

In summary, we demonstrate that highly stable surface peroxo units result from the adsorption of atomic oxygen onto flat undefective surfaces and onto one-electron defects, as well as from the vacancy annihilation process by O_2 and O_2^- molecules. These peroxide units are predicted to be abundant both on oxidized and reduced surfaces. Due to the high barrier for diffusion, atomic O mobility is not activated in the low-temperature oxidation regime ($<200\,^\circ$C). Molecular oxygen is shown to be almost unbound on oxidized surfaces, to rapidly seal vacancy sites, and to be weakly bound to one-electron defect sites. The binding of superoxiodes displays strong surface selectivity, being governed by the electrostatic interaction with surface Ce^{4+} ions, and being at the basis of the higher reactivity of nanocrystalline ceria. The calculated stretching frequencies for the O_2^- species allows for a direct association of the specific peaks at 1123–1135 cm^{-1} to the reactive species controlling low-temperature oxidation reactions on ceria. These results point to the general importance of charge-transfer processes at the interface between metal oxides, oxygen adsorbates, and supported metal particles, and are going to be relevant to a broader class of metal-oxide surfaces.

We are grateful to S. Baroni, F. Esch, S. de Gironcoli, and G. Balducci for useful discussions. Computer time from the INFM-CNR progetto calcolo parallelo is acknowledged.

[1] M. Valden, X. Lai, and D. W. Goodman, Science **281**, 1647 (1998).
[2] Q. Fu, H. Saltsburg, and M. Flytzani-Stephanopoulos, Science **301**, 935 (2003).
[3] E. Wahlstrom, N. Lopez, R. Schaub, P. Thostrup, A. Ronnau, C. Africh, E. Laegsgaard, J. K. Norskov, and F. Besenbacher, Phys. Rev. Lett. **90**, 026101 (2003).
[4] J. Guzman, S. Carrettin, and A. Corma, J. Am. Chem. Soc. **127**, 3286 (2005).
[5] *Catalysis by Ceria and Related Materials*, edited by A. Trovarelli (Imperial College Press, London, 2002).
[6] F. Esch, S. Fabris, L. Zhou, T. Montini, C. Africh, P. Fornasiero, G. Comelli, and R. Rosei, Science **309**, 752 (2005).
[7] S. Gritschneder, Y. Namai, Y. Iwasawa, and M. Reichling, Nanotechnology **16**, 41 (2005).
[8] S. Fabris, G. Vicario, G. Balducci, S. de Gironcoli, and S. Baroni, J. Phys. Chem. B **109**, 22860 (2005).
[9] M. Nolan, S. Grigoleit, D. Sayle, S. C. Parker, and G. W. Watson, Surf. Sci. **576**, 217 (2005).
[10] A. N. Il'ichev, M. D. Shibanova, A. A. Ukharskii, A. M. Kulizade, and V. N. Korchak, Kinet. Katal. **46**, 387 (2005).
[11] V. V. Pushkarev, V. I. Kovalchuk, and J. L. d'Itri, J. Phys. Chem. B **108**, 5341 (2004).
[12] S. Baroni, A. Dal Corso, S. de Gironcoli, and P. Giannozzi, http://www.pwscf.org
[13] H. Jónsson, G. Mills, and K. W. Jacobsen, *Classical and Quantum Dynamics in Condensed Phase Simulations* (World Scientific, Singapore, 1998), Chap. 16, p. 385.
[14] S. Fabris, S. de Gironcoli, S. Baroni, G. Vicario, and G. Balducci, Phys. Rev. B **71**, 041102(R) (2005).
[15] G. Geneste, J. Morillo, and F. Finocchi, J. Chem. Phys. **122**, 174707 (2005).
[16] C. D. Valentin, R. Ferullo, R. Binda, and G. Pacchioni, Surf. Sci. **600**, 1147 (2006).
[17] H. L. Tuller and A. S. Nowick, J. Phys. Chem. Solids **38**, 859 (1977).
[18] K. M. Ervin, I. Anusiewicz, P. Skurski, J. Simon, and W. C. Lineberger, J. Phys. Chem. A **107**, 8521 (2003).